

# Analysis of Effects of Sizes of Orifice and Pockets on the Rigidity of Hydrostatic Bearing Using Neural Network Predictor System

**Fazıl Canbulut, Cem Sinanoglu, Şahin Yildirim**

*Erciyes University, Faculty of Eng., Mechanical Engineering Department,  
Kayseri, 38039, Turkey*

This paper presents a neural network predictor for analysing rigidity variations of hydrostatic bearing system. The designed neural network has feedforward structure with three layers. The layers are input layer, hidden layer and output layer. Two main parameter could be considered for hydrostatic bearing system. These parameters are the size of bearing pocket and the orifice dimension. Due to importance of these parameters, it is necessary to analyse with a suitable optimisation method such as neural network. As depicted from the results, the proposed neural predictor exactly follows experimental desired results.

**Key Words :** Hydrostatic Bearing, Orifice Dimension, Neural Predictor

## Nomenclature

$P_c$  : Pocket pressure  
 $R_d$  : Outer radius of slipper  
 $R_i$  : Inner radius of slipper  
 $\bar{P}$  :  $= P_p/P_c$  non-dimensional pressure  
 $P$  : Pressure  
 $P_p$  : Supply pressure  
 $Q_c$  : Leakage from pool across slipper lands  
 $Q_r$  : Radial direction flow rate  
 $\eta$  : Dynamic viscosity  
 $d_e$  : Diameter of orifice  
 $l_c$  : Length of orifice  
 $k_c$  : Orifice coefficient  
 $\bar{h}$  :  $= h/R_d$  non-dimensional clearance  
 $k$  : Bearing rigidity  
 $\bar{k}$  :  $= k/P_p R_d$  non-dimensional bearing rigidity  
 $\bar{W}$  :  $= W/P_p R_d^2$  non-dimensional vertical load

$\bar{R}$  :  $= R_d/R_i$  non-dimensional radius  
 $E(\bar{\omega})$  : Error variations for weights  
 $f(x)$  :  $= \frac{1}{1+e^{-x}}$  logistic function  
 $\mu$  : Momentum  
 $\eta_i(t)$  : Learning rate  
 $\bar{\delta}(t)$  : Exponential average of past value of  $\delta$   
 $\delta(t)$  : Derivation of error in weights  
 $t$  : Time  
 $K$  : Constant value for learning rate  
 $\phi$  : Correction factor of learning rate  
 $\theta$  : Coefficient of the exponential average value  
 $\Delta(\bar{\omega})$  : The weights variations after update  
 $n_o$  : Numbers of output units  
 $n_H$  : Numbers of hidden units  
 $n_i$  : Numbers of input units  
 $R$  : Radius  
 $\bar{R}^*$  : Inverse dimensionless radius  
 $u_i$  : Output signals of hidden layer  
 $f(.)$  : Simple non-linear function  
 $h$  : Clearance  
 $W$  : Vertical load  
 $S(t)$  :  $= \frac{\partial E}{\partial \bar{\omega}}(t)$   
 AF : Activation function

\* Corresponding Author.

**E-mail :** canbulut@erciyes.edu.tr

**TEL :** +0090-352-4374901-32078

**FAX :** +0090-352-4375784

Erciyes University, Faculty of Eng., Mechanical Engineering Department, Kayseri, 38039, Turkey. (Manuscript Received July 8, 2003; Revised December 26, 2003)

N : Training numbers

## 1. Introduction

Piston pumps are manufactured two types of radial and axial. Also, produced with different capacity, for producing fluid with variable pressure. The most common method of lubricating the slippers is to use the oil in the pump and to generate pressure under the slipper in order for the slippers to float on an oil film. This lifting pressure can be generated entirely hydrodynamically. Alternatively, the lift can be obtained largely hydrostatically by tapping the piston pressure.

Circular pocket hydrostatic axial bearings in hydraulic axial piston pump are under the influence of a wide variety of forces. Therefore, the sliding surface of hydrostatic bearing must have the necessary axial rigidity. The constitution of the slope of load film thickness curve is quite important for hydrostatic bearing applications. The value of this slope called rigidity is capability of the bearing to withstand the variation in the load depending on the variation of film thickness. The bearing rigidity is one important factor in selecting parameters of the bearing working under variable loads. Therefore, the bearing must be designed in such a way as to obtain maximum rigidity in minimum oil film thickness and maximum load. The surface roughness and sudden load are two important factors to decrease oil film thickness. Oil film permanency is only possible when adequate oil is supplied to the hydrostatic bearing pocket. Lubrication oil is transferred to bearing pocket by orifice and flow-control valve in hydrostatic axial bearing. In addition to these factors, bearing rigidity is affected by the size of the pocket.

Koç and Hooke have examined the design of hydrostatically balanced bearings as used in the slippers of high pressure axial pumps, and outlined a design procedure whereby the slipper behaviour, minimum film thickness and loss of high pressure fluid could be estimated. It was shown that for successful operation the slippers need to have small amounts of non-flatness on

the running surfaces. In addition, good agreement between the measured and calculated film thickness was demonstrated (Koç and Hooke, 1997).

The same researchers experimentally investigated the performance of hydrostatic slipper bearings in axial piston pumps and motors (Koç and Hooke, 1996). The effect of clamping ratio, offset loading and orifice size on the behaviour of overclamped and underclamped slippers was outlined. It was shown that the slippers run satisfactorily with no orifice and have their greatest resistance to tilting couples and to minimum film thickness. The underclamped slippers and slippers with larger orifice diameter run with relatively larger clearance and tilt than those of overclamped slippers with no orifice. Cavitation tends to affect the slippers, especially at the rear of the slipper. Ineffective flood lubrication might be the cause of the cavitation and oil jet pressure must have maintained to prevent oil starvation. In high pressure hydraulic equipment the bearings and seals are usually designed to operate hydrostatically in partial. In some, such as the end plates or bushes of gear pumps and the valve plates of axial piston pumps, this is achieved by adjusting the pressurised areas so that the hydrostatic loads are nearly in balance, leaving a small residual clamping load to be carried by hydrodynamic pressures (Koç, 1989).

Wang and Yamaguchi presented the characteristics of disk-type hydrostatic thrust bearings supporting concentric loads, simulating the major bearing/seal parts of water hydraulic pumps and motors (Wang and Yamaguchi, 2002a). They evaluated the characteristics by studying the relationships among the load carrying capacity, pocket pressure, film thickness, and leakage flow rate.

Wang and Yamaguchi also theoretically investigated the load carrying capacity, power losses and stiffness of disk-type hydrostatic thrust bearings including the case of eccentric load for elastic and rigid materials respectively (Wang and Yamaguchi, 2002b). In their paper, a numerical analysis method was employed based on a two-dimensional elastohydrostatic problem with elas-

tic deformation model.

Another approach for different lubricant and lubrication condition can be given in (Durak, 2003). An experimental investigation has been presented for the performance of porous bearing under different lubricating conditions. The experimental results obtained in his study indicated that the correct selection of lubricant and suitable running conditions.

In this study, the effects of orifice diameter and the size of pocket in slippers with circular pocket, which affect the performance of swash plate axial piston pump and motor are examined using neural network. The neural network is employed as a robust predictor for analyzing hydrostatic bearing systems instead of traditional optimization methods. The neural network has fast learning and parallel processing structure.

### 2. Theoretically Analyses

Figure 1 shows typical hydrostatic bearing and plate system used in this study. As can be seen in the figure, the slipper moves on slipper plate with a certain film thickness ( $h$ ). The fluid coming from piston side is transferred to the pocket (bottom of the slipper) by orifice to equilibrate the slipper. While the system is running, the clearance ( $h$ ) between the slipper and the slipper plate must be neither small enough to cause metal-metal contact nor too big to cause fluid leakage. Therefore, this critical area has to be precisely designed in consideration of the dynamic working conditions.

The vertical load  $W$  (Fig. 1) acting on circular pocket hydrostatic bearing and formed by loading pressure  $P_p$  is kept in equilibrium by the fluid pressure between the load bearing face and the opposite element.

The vertical load (Canbulut et al., 1992) is

$$W = \frac{\pi P_c (R_d^2 - R_i^2)}{2 \ln(R_d/R_i)} \tag{1}$$

where,  $P_c$  is pocket pressure,  $R_d$  and  $R_i$  are outer and inner radii of bearing respectively.

The flow-rate ( $Q_c$ ) transferred from loading

area of the bearing to bearing pocket and the radial direction flow-rate ( $Q_r$ ) neglecting the speed of the hydrodynamic bearing are

$$Q_c = \frac{\pi d_c^4}{128 \eta l_c} (P_p - P_c) \tag{2}$$

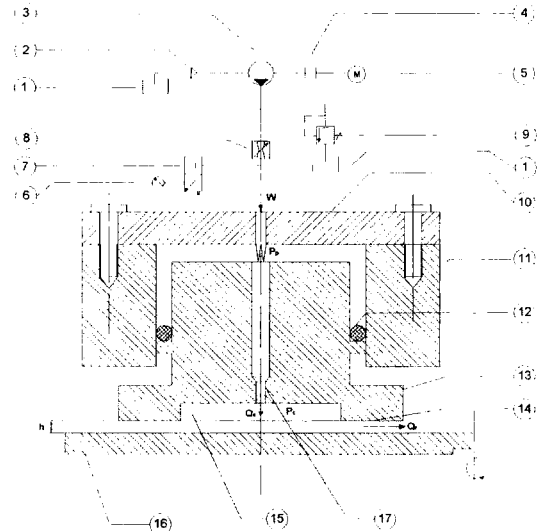
and

$$Q_r = \frac{P_c \pi h^3}{6 \eta \ln(R_d/R_i)} \tag{3}$$

respectively, where  $d_c$  and  $l_c$  are the diameter and length of orifice,  $\eta$  is the dynamic viscosity of oil.

If  $P_c$  is derived from Eq. and substituted into Eq., we obtain

$$W = \frac{3 Q_r \eta (R_d^2 - R_i^2)}{h^3} \tag{4}$$



Part No	Part Name
1	oil tank
2	filter
3	pump
4	coupling
5	motor
6	manometer
7	pressure control valve
8	flow control valve
9	pressure relief valve
10	cylinder cover
11	cylinder block
12	O-ring
13	slipper
14	hydrodynamic bearing area
15	hydrostatic pocket
16	slipper plate
17	orifice

Fig. 1 Typical hydrostatic slipper and circuit elements

If the fluid permanency is considered ( $Q_c=Q_r$ ) and Eq. is placed to Eq., the load expression becomes independent of viscosity

$$W=3\pi \frac{k_c}{h^3} P_p \left(1-\frac{1}{\bar{P}}\right) R_d^2 \left(1-\frac{1}{\bar{R}^2}\right) \quad (5)$$

where,  $\bar{P}=P_p/P_c$ ,  $k_c=d_c^2/128.l_c$ , and  $\bar{R}=R_d/R_i$ .

Generally, the rigidity of hydrostatic bearing system is denoted by

$$k=-\frac{dW}{dh} \quad (6)$$

The negative sign (-), is written to signify the positivity of rigidity equilibrium not in mathematical sense. Rigidity ( $k$ ) can be driven in the following form from the Eq. regarding to derivative of  $h$  film thickness

$$k=3 \frac{W}{h} \quad (7)$$

If necessary for the sake of the simplicity in working with dimensionless values, the bearing rigidity in dimensionless form can be expressed as follows

$$\bar{k}=3 \frac{\bar{W}}{\bar{h}} \quad (8)$$

where in  $\bar{h}=h/R_d$ ,  $\bar{W}=W/R_p R_d^2$ ,  $\bar{k}=k/P_p R_d$ .

### 3. Experimental System

#### 3.1 Experimental setup

Parameters governing the workings of the hydrostatic sliding bearing precedently mentioned can be explained theoretically with certain assumptions, but experimental determination of the values closest to reality is the most favorable scientific approach.

In this study, the effects of slippers, which enhance the efficiency of axial piston pumps and motors on lubrication are examined under various working conditions. An experimental setup has been designed to examine the performance of slippers, in various working conditions of the axial piston pump. The schematic experimental setup is shown in Fig. 2.

Experimental setup consists of three main units: The main test unit, for the testing of slippers, the hydraulic power unit and the driving unit

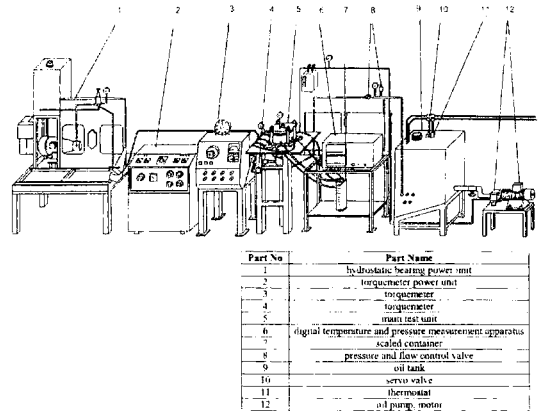
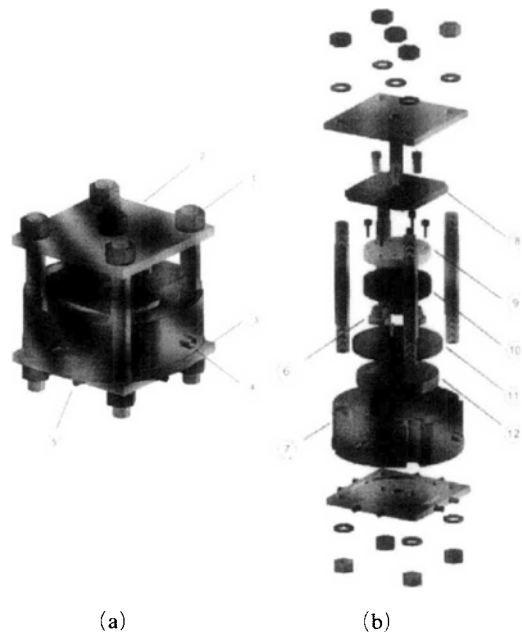


Fig. 2 The schematic experimental setup



Part No	Part Name
1	stud bolts
2	top table
3	bottom table
4	slipper leakage oil exit
5	hydrostatic bearing oil exit
6	slipper
7	oil barricade
8	moving plate in vertical direction
9	cylinder cover
10	cylinder block
11	slipper plate
12	hydrostatic bearing

Fig. 3 The main setup

with control and measurement devices.

### 3.2 Main test unit

The slippers in axial piston pumps and motors working on the hydrostatic bearing principle were taken into account in this study. The structure of the main test unit are demonstrated in Fig. 3.

This unit consists of the bottom (3) and top tables (2), which are constant with studs and stud bolts (1), the hydraulic loading cylinder (block) (10), slippers (6) and the elements providing non-leakage (7). The hydrostatic bearing with a large circular pocket has been put up on the bottom table to operate the slipper plate (11) smoothly. The loading cylinder was designed such a way to load three slippers simultaneously.

This region is classified in captions as first, hydrostatic bearing and slipper plate, second, hydraulic loading cylinders and slippers, third, leakproof.

#### 3.2.1 Hydrostatic bearing and slipper plate

Since they instantly resist sudden increases of load, hydrostatic bearings enable the moving components on them to work more steadily. A hydrostatic bearing with a circular pocket has been provided for the slipper plate, which is in relative motion with slippers, to work without vibration. The slipper plate moved by a shaft from the gearbox is on the hydrostatic bearing (No 11 in Fig. 3). The slipper plate is designed in such a way as to prevent the mixture of oil coming from the hydrostatic bearing with the oil from the slipper plate. The surfaces of the slipper plate which are responsible for slipping are ground to surface roughness quality of  $0.6 \mu\text{m}$ . The angular eccentricity is  $25 \mu\text{m}$ .

#### 3.2.2 Hydraulic cylinder and slipper

There are three cylinder barrels ( $\varnothing 25.5 \text{ mm}$ ) on the hydraulic loading cylinder (Part No 10 in Fig. 3) to position the slipper at an angle of  $120^\circ$ . The connections in the cylinder are designed in such a way as to allow each slipper to be loaded equally. The loading pressure is controlled by a

manometer on cylinder cover.

The pressure measurement located on the bottom sliding surface of the slippers with an outer diameters of  $\varnothing 41 \text{ mm}$ . Slippers are made of brass material and given tolerances their regions on the cylinder block supplying leakproof. Moreover, the surface roughness of sliding side on the slipper plate are processed with different values to aim of the experiments. The orifices with inner diameters  $0.3 \text{ mm}$ ,  $0.5 \text{ mm}$  are used to send the oil from top region to slipper pocket.

#### 3.2.3 Leakproof

Oil barricade made of cast aluminium is used to prevent mixture each other between the leakage oil bottom the slippers and oil get out of hydrostatic bearing (Part No 7 in Fig. 3). Experimental set is supplied with two hydraulic power units. One of them, it is supplied to hydrostatic bearing (Part No 12 in Fig. 3) to prove regular working of slipper plate, another is supplied to load slippers in the cylinder block and support oil of slipper pocket.

### 3.3 Experimental method

In the experiment, three circular pocket bearings with different diameters have been tested. The Bourdan type hydrostatic pressure manometers were used to measure the loading pressure, pocket pressure and the pressures of the front and rear sliding faces where considered to be hydrodynamic effect occurs. Oil temperature was set to be constant to prevent the variation of viscosity.

The ambience temperature was held at  $20^\circ\text{C}$ . Moreover, the temperature of the oil used in the experiments at the beginning of experiment was considered not to exceed  $20^\circ\text{C}$ . Therefore, an air-cooled system was used for keeping the temperature constant.

Loading force can be obtained from the piston diameter ( $\varnothing 29.85 \text{ mm}$ ) and measured loading pressure ( $p_p$ ). Film thickness ( $h$ ) can be found by using Eq. (3) consisting of geometric dimensions ( $R_a$ ,  $R_i$ ), measured pocket pressure ( $p_c$ ) and dynamic viscosity. Finally, bearing rigidity ( $k$ ) can be estimated by using Eq. (7).

### 4. Artificial Neural Networks

Artificial neural networks (ANNs) have a large number of highly interconnected processing elements (nodes or units) that usually operate in parallel and are configured in regular architectures. The collective behaviour of an ANNs, like a human brain, demonstrates the ability to learn, recall, and generalise from training patterns or data. ANNs are inspired by modelling networks of real (biological) neurons in the brain. Hence, the processing elements in ANNs are also called “artificial neurons”, or “simply neurons” (Sinanoglu, 2004).

A typical real neuron has a branching dendritic tree that collects signals from many other neurons in a limited area; a cell body that integrates collected signals and generates a response signal and along branching axon that distributes the response through contacts with dendritic trees of many other neurons. The response of each neuron is a relatively simple non-linear function of its inputs and is largely determined by the strengths of the connections from its inputs.

An ANNs shown in Fig. 4 is very loosely based on these ideas. In the most general terms, a ANNs consist of large number of simple processors linked by weighted connections. A network is specialised different functions by varying the connection topology and the values of the

connecting weights. Complex functions can be implemented by connecting units together with appropriate weights. Usually, the processing units have responses like (see Fig. 4)

$$y=f\left(\sum_i u_i\right) \tag{9}$$

where  $u_i$  are the output signals of hidden layer to output layer,  $f(\cdot)$  is a simple nonlinear function such as the sigmoid, or logistic function. This unit computes a weighted linear combination of its inputs and passes this through the nonlinearity to produce a scalar output.

A network is trained so that application of a set inputs produces the desired set of outputs. The proposed neural network was trained with two types of learning algorithms which are QuickProp and Delta-Bar-Delta. Quick propagation is based on the following assumptions (Sinanoglu et al., 2004; Canbulut et al., 2004).

$E(\bar{\omega})$  for each weight can be approximated by a parabola that opens upward, and the change in slope of  $E(\bar{\omega})$  for this weight is not affected by all other weights that change at the same time. The weight update rule is:

$$\Delta\bar{\omega}(t)=\frac{S(t)}{S(t-1)-S(t)}\Delta\bar{\omega}(t-1)-\eta_i S(t) \tag{10}$$

where

$$S(t)=\frac{\partial E}{\partial \bar{\omega}}(t) \tag{11}$$

The numerator is the derivative of the error with respect to the weight and  $(S(t-1)-S(t))/\Delta\bar{\omega}(t-1)$  is a finite difference approximation of the second derivative. Together these approximate Newton’s method for minimising a one dimensional function

$$f(x): \Delta x=-f'(x)/f''(x) \tag{12}$$

To avoid taking an infinite backward step, or a backward uphill step, a maximum growth factor parameter  $\mu$  is introduced. No weight change is allowed to be larger than  $\mu$  times the previous weight change. Quick propagation has a fixed learning rate parameter,  $\eta_i$ , that needs to be chosen to suit the problem.

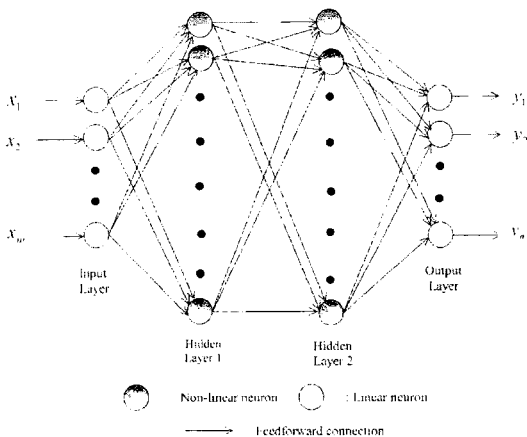


Fig. 4 A layered feed-forward artificial ANNs

An adaptive learning rate method (Delta-Bar-Delta) (Yıldırım and Uzmay, 2003; Yıldırım, 2002) in which every weight has its own learning rate. The learning rates are updated based on the sign of the gradient. If the gradient does not change signs on successive iterations then the step size is increased linearly. If the gradient changes signs, the learning rate is decreased exponentially. In some cases this method seems to learn much faster than non-adaptive methods. Learning rates  $\eta_i(t)$  for delta-bar-delta algorithm are updated as follows :

$$\Delta\eta_i(t) = \begin{cases} K & \text{if } \bar{\delta}(t-1)\delta(t) > 0 \\ -\phi\eta_i(t) & \text{if } \bar{\delta}(t-1)\delta(t) < 0 \\ 0 & \text{else} \end{cases} \quad (13)$$

where  $\delta(t) = \frac{\partial E}{\partial w}$  at time  $t$  and  $\bar{\delta}$  is the exponential average of past values of  $\delta$ .

$$\bar{\delta}(t) = (1-\theta)\delta(t) + \theta\bar{\delta}(t-1) \quad (14)$$

where  $\delta(t)$  is the derivation of error in weights and  $\theta$  is the coefficient of the exponential average value.

The activation (transfer) functions are possible for each hidden layer and the output layer. In this study, the logistic function is used to hidden layers and output layers. Linear function is taken for input layer. The logistic function is used to hidden layers and output layers as an activation function. Logistic function is as follows ;

$$y = f(x) = \frac{1}{1 + e^{-x}} \quad (15)$$

Linear function is taken for input layer. The linear function is ;

$$y = f(x) = x \quad (16)$$

The result is given in the RMS form for comparison with experimental (desired) results (Table 1). The structural and training parameters of the network are given in Table 2.

Figure 5 shows the currently loaded network. The connections can represent the current weight values for each weight. Squares represent input nodes, circles depict the neurons, the rightmost being the output layer. Triangles represent the bias for each neuron. The neural network consist

of three layer which are input, output and hidden layers. It is easy train the neural network using

**Table 1** Average and maximum Rms error for training algorithms used

		Training Algorithms	
		Quick Prop	Delta-Bar-Delta
Case 1 Figure 6	Average RMS	0.0458435	0.101273
	Maximum RMS	0.0999992	0.221908
Case 2 Figure 7	Average RMS	0.0450971	0.0603726
	Maximum RMS	0.0984351	0.0998888
Case 3 Figure 8	Average RMS	0.0704097	0.0705123
	Maximum RMS	0.0995733	0.0992878
Case 4 Figure 9	Average RMS	0.0737403	0.0706576
	Maximum RMS	0.0999829	0.0999235
Case 5 Figure 10	Average RMS	0.0523453	0.0662205
	Maximum RMS	0.0999353	0.0999115

**Table 2** Structural and training parameters of the proposed neural predictor

	$\eta_i$	$\mu$	$N$	$n_I$	$n_H$	$n_o$
Case 1 Figure 6	0.1	0	200000	1	10	3
Case 2 Figure 7	0.1	0	200000	1	10	3
Case 3 Figure 8	0.1	0	200000	1	10	3
Case 4 Figure 9	0.1	0	200000	1	10	3
Case 5 Figure 10	0.1	0	200000	1	10	4

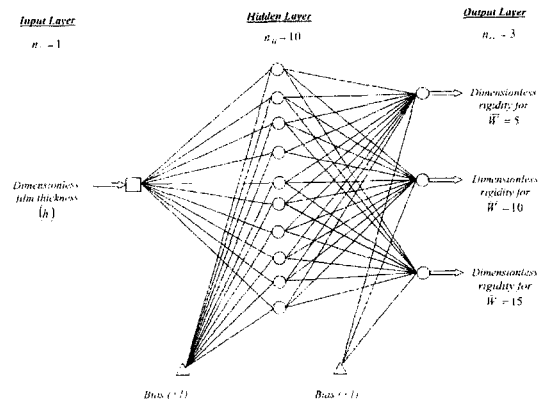


**Fig. 5** Currently loaded network

one input and three outputs. The input and outputs data are used as learning and testing data. But the testing data samples are decreased from learning rate.

### 5. Simulation Results

The bearing rigidity has been examined in the framework of the analyses above in various sizes of orifice and pocket. The variation of dimensionless bearing rigidity with dimensionless film thickness in various dimensionless bearing load for desired and neural network approaches is given in Fig. 6 (Case 1). It is seen that the rigidity of bearing is greater for the lower values of film thickness and higher values of load. The load and film thickness does not much affect rigidity after a certain film thickness. The results in the ANNs and test data targets (experiments) are match for different dimensionless bearing load. ANNs system can easily predict bearing rigidity parameters for real time application.

Figure 7 (Case 2) shows the results of desired and neural network assuming the variation of the dimensionless bearing rigidity with dimensionless bearing load in various dimensionless film thickness. The dimensionless bearing rigidity is linearly increased with increased dimensionless bearing load ( $\bar{W}$ ). It is seen that the rigidity of bearing is greater for the lower values of film thickness and higher values of load. The load and film thickness does not much affect rigidity after a certain bearing load. The bearing rigidity was

examined in various dimensionless film thickness, while the bearing rigidity rose from to , and the capacity of load and dimensionless film thickness were change. While the bearing rigidity falls swiftly down to value of dimensionless bearing load, after this point the fall is less swift.

In case 2, neural network predictor consisted of one input neurone, ten hidden layer neurones, three output neurones with logistic non-linear activation function. Network has good performance to predict such systems with all kinds of working conditions.

The bearing geometry, orifice diameter, and the levels of loading and pocket pressures in dynamic working can be evaluated in the oil film equation, independent of viscosity. The effects of two factors on the rigidity of hydrostatic bearing have been investigated experimentally. These factors are orifice diameter and bearing ratio. The orifice diameter and bearing ratio are considered two different levels ( $d_c=0.3$  mm,  $d_c=0.5$  mm) and three different levels ( $\bar{R}=1.650$ ,  $\bar{R}=1.422$ ,  $\bar{R}=1.784$ ) respectively (Canbulut et al., 1992).

The variation of bearing rigidity with dimensionless radius ratios, in various loading pressures is shown in Fig. 8 (Case 3). As can be seen in the figure, the bearing rigidity is increased with loading pressure at the same radius ratios.

The load equilibrium on sliding faces is supplied predominantly by hydrostatic bearing in the lower radius ratios. As the bearing pocket shrinks, this weight ratio slips towards hydrodynamic bearing area and thus increases rigi-

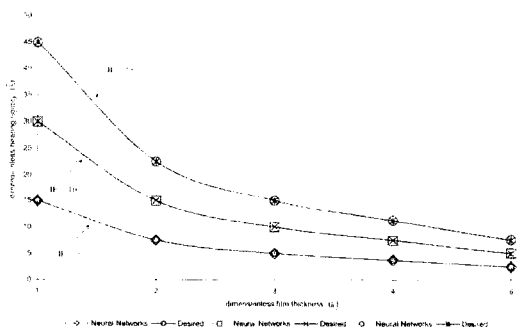


Fig. 6 The relationship between dimensionless bearing rigidity and dimensionless film thickness

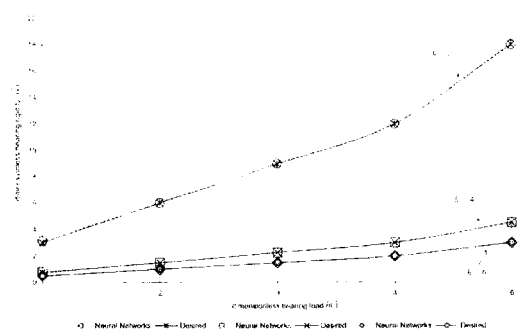


Fig. 7 The relationship between dimensionless bearing rigidity and dimensionless bearing load

dity. It is suitable that the radius ratio should be selected around  $R=1.5$ , since no significant change in the bearing rigidity is observed, when  $R$  ranges from 1.422 to 1.650, and since they are consistent with the findings from theoretical values. The bearing rigidity is also increased with increases loading pressure because of the augmentation of the  $P_c/P_p$  ratio. The designed neural predictor has also superior performance for modelling of such systems.

Figure 9 (Case 4) shows the variation of film thickness with dimensionless radius in various loading pressure. The film thickness is also increased with increased dimensionless radius ratio especially after  $R=1.65$ . The hydrodynamic bearing area is effective to support load with decreasing area. Therefore, this area must produce the pressure necessary for the equilibrium of the load. Since, however, it is possible only with

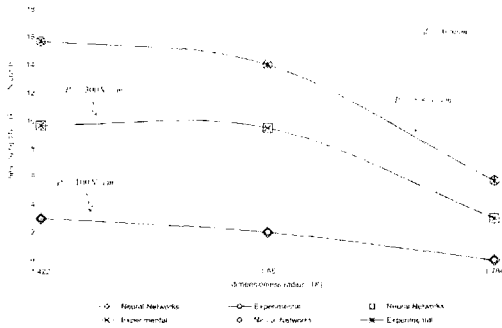


Fig. 8 The relationship between bearing rigidity and dimensionless radius

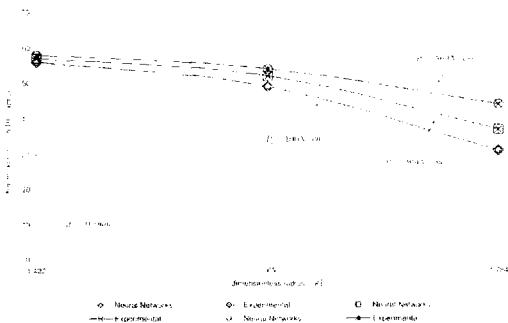


Fig. 9 The relationship between film thickness and dimensionless radius

small film thickness, the variation corroborates theoretical results also. The results in the ANNs and test data targets (experiments) are similar to each other in both approaches. The film thickness can be predicted using ANNs for experimental approach.

The effects of various orifice diameters and radius ratios on the system performance have been examined and a behaviour similar to the one in Fig. 10 (Case 5) has been observed. As can be seen in the figure, generally, the augmentation of loading pressure linearly increases bearing rigidity in two various orifice diameters and radius ratios. When the diameter of orifice decreased, the linear flow increased. Otherwise, the diameter of orifice is increased, the linearity of flow decreased.

Especially when, the diameter of orifice is 0.3 mm and the radius ratios are 1.67 and 1.784, increasing loading pressure caused rigidity to show fluctuating changes. In this curve, as the pressure increased to 200 N/cm<sup>2</sup> and 400 N/cm<sup>2</sup>, rigidity decreased. This was believed to have resulted from faulty measurement. The behaviour posed by these curves is the form of behaviours expected theoretically. As shown in this figure, the results obtained from these two approach are consistent with each other for different working conditions such as orifice diameter, dimensionless radius and loading pressure.

The error convergence graphs of the Case 1, 2, 3, 4 and 5 are depicted in Fig. 11, 12, 13, 14 and 15 during the training of the network. As can be

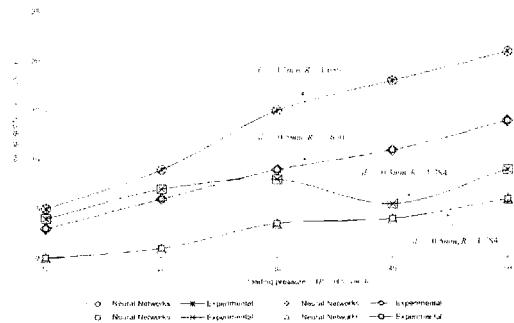


Fig. 10 The relationship between bearing rigidity and loading pressure

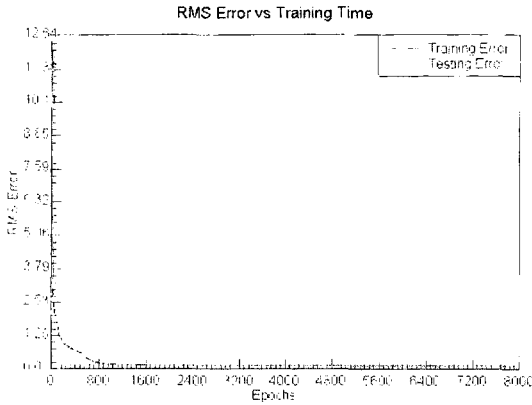


Fig. 11 The error convergence graph of the Case 1

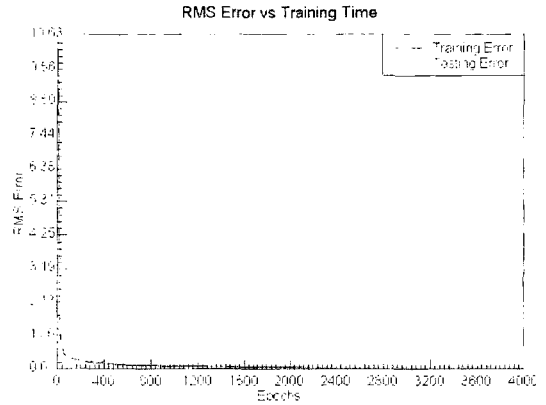


Fig. 14 The error convergence graph of the Case 4

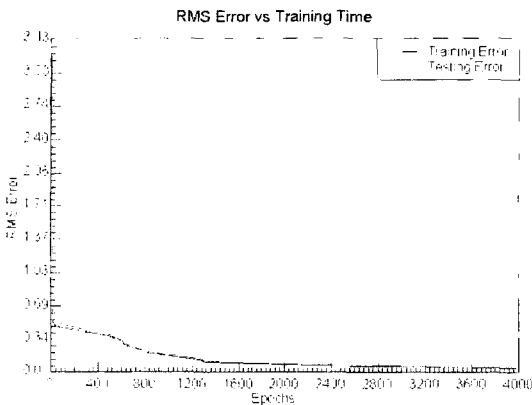


Fig. 12 The error convergence graph of the Case 2

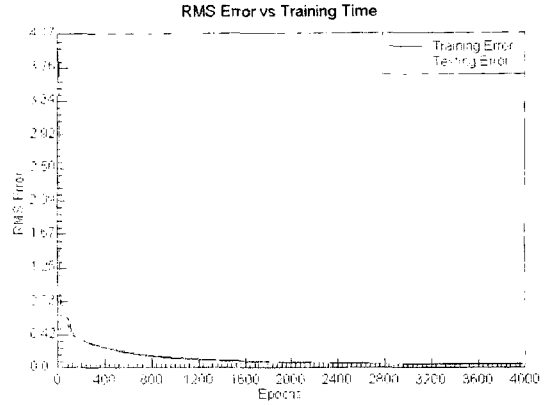


Fig. 15 The error convergence graph of the Case 5

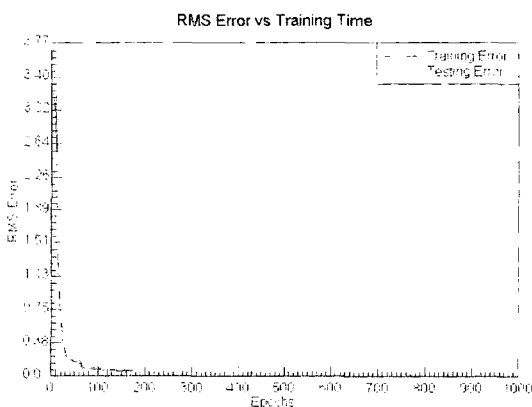


Fig. 13 The error convergence graph of the Case 3

seen from the figures, the error is rapidly reduced to small values. Small epochs can be employed for Case 3. But Case 1 needs comparatively large

number of epochs, because of sudden decreased film thickness.

## 6. Conclusions

In this paper, an experimental and neural network application were employed for analysing rigidity variations on hydrostatic bearing system. As can be depicted from the results, the neural predictor can be used as a predictor for possible experimental applications of hydrostatic bearing system. Also, on the different working conditions of the system, neural network exactly followed the rigidity variations of the system with various loading pressure and dimensionless radii.

It was shown from theoretical and experimental results that orifice diameter and radius ratio significantly affect on bearing rigidity. The design

criteria of an orifice diameter of 0.3 mm and a radius ratio of about 1.5 can be recommended for the procurement of maximum rigidity.

Finally, due to the parallel structure and fast learning of neural network, this kind of neural network algorithm could be utilised to model another types of bearing systems. The neural network can be used in practical applications after finding exact model of the system.

## References

- Canbulut, F., Sinanoğlu, C. and Yıldırım, Ş., 2004, "Neural Network Analysis of Leakage Oil Quantity In The Design of Partially Hydrostatic Slipper Bearings," *Industrial Lubrication and Tribology*, (in press).
- Canbulut, F., Koç, E. and Canbulut, F., 1992, "The Effects of Sizes of Capillary Tube and Pockets on the Rigidity of Hydrostatic Bearing," *5th. National Machine Design and Manufacturing Congress*, ODTU, Turkey.
- Durak, E., 2003, "Experimental Investigation of Porous Bearings Under Different Lubricant and Lubricating Conditions," *KSME International Journal*, Vol. 17, No. 9, pp. 1276~1286.
- Koç, E., 1989, "Analytical and Experimental Investigation into the Sealing and Lubrication Mechanism of the Gear ends in Pumps," *Wear*, Vol. 135, pp. 79~94.
- Koç, E and Hooke, C. J., 1996, "Investigation into the Effects of Orifice Size, Offset and Overclamp Ratio on the Lubrication of Slipper Bearings," *Tribology International*, Vol. 29, No. 4, pp. 299~305.
- Koç, E. and Hooke, C. J., 1997, "Considerations in the Design of Partially Hydrostatic Slipper Bearings," *Tribology International*, Vol. 30, pp. 815~823.
- Sinanoğlu, C, Kurban, A. O. and Yıldırım, Ş., 2004, "Analysis of Pressure Variations on Journal Bearing System Using Artificial Neural Network," *Industrial Lubrication and Tribology*, (in press).
- Sinanoğlu, C., 2004, "The Analysis of The Effects of Surface Texture on The Capability of Load Carriage of Journal Bearings Using Neural Network," *Industrial Lubrication and Tribology*, (in press).
- Wang, X. an Yamaguchi, A., 2002a, "Characteristics of Hydrostatic Bearing/Seal Parts for Water Hydraulic Pumps and Motors. Part 1 : Experiment and Theory," *Tribology International*, Vol. 35, pp. 425~433.
- Wang, X. and Yamaguchi, A., 2002b, "Characteristics of Hydrostatic Bearing/Seal Parts for Water Hydraulic Pumps and Motors. Part 2 : On Eccentric Loading and Power Loses," *Tribology International*, Vol. 35, pp. 435~442.
- Yıldırım, Ş. and Uzmay, I., 2003, "Neural network applications to vehicle's vibration analysis," *Mechanism and Machine Theory*, Vol. 38, pp. 27~41.
- Yıldırım, Ş., 2002, "Robot Trajectory Control Using Neural Networks," *IEE Electronics Letters*, Vol. 38, No. 19, pp. 1111~1113.